Understanding the miscibility of polyoxymethylene dimethyl ethers (OME_n) and diesel blend using molecular dynamics simulation

Mengwei Yu, Cheng Chen, Xi Jiang*

School of Engineering and Materials Science,

Queen Mary University of London,

Mile End Road, London E1 4NS, UK

*Corresponding author. Email: xi.jiang@qmul.ac.uk

Abstract

Polyoxymethylene dimethyl ethers (OME_n) as an alternative fuel have attracted considerable interest in recent years, owing to their much reduced environmental impact. Since OME_n is often blended with diesel, the miscibility and stability of OME_n/diesel mixtures are important for engine operation. In this study, molecular dynamics method was used to investigate the miscibility of OME_{1-6} and diesel blends. The results suggest that the miscibility of OME_n and diesel blends decreases with the increasing number of oxymethylene units. The aromatics and heteroatomic molecules help maintain the stability of OME_n/diesel blends. The intermolecular interactions between OME_{1-6} and diesel molecules were investigated, which revealed that the electrostatic interaction plays a significant role in the liquid–liquid equilibrium of OME_n/diesel blends. The molecules in diesel having strong electrostatic interaction with OME_n are prone to accumulate around OME_n. The electrostatic interaction between diesel and OME_n molecules depends on the molecular structure and electronegativity differences of atoms in diesel molecules. The analyses of MD results coupled to minimum-distance distribution functions show an accumulation of paraffins and naphthenes close to OME_n at ~2.36 Å, and suggest a strong interaction of OME_n with diesel carbazole molecules via hydrogen bonds. The results also indicate that the chain length and structure of alkanes have little impact on the molecular distribution around OME_n.

Keywords: polyoxymethylene dimethyl ethers; diesel; molecular dynamics; simulation; miscibility.

Abbreviations (for chemicals)

ANT	anthracene	DMO	2,4-dimethyloctane
CAR	carbazole	EIC	eicosane
DBT	dibenzothiophene	MET	2-methyltetradecane
DCP	*n*-decylcyclopentane	NAP	naphthalene
DEC	*n*-decane	NCH	*n*-nonylcyclohexane
DHN	decahydronaphthalene	OME_n	polyoxymethylene dimethyl ethers
DME	dimethyl ether	PEN	*n*-pentadecane

1. Introduction

To address climate change and other environmental concerns, decarbonisation is urgently needed for the energy sector, which has been relying on fossil fuels for many decades. However, there are difficult-to-decarbonise industries such as sea and air transport. Diesel fuels have been broadly used in large marine engines due to their superior energy density and stability. However, the particulate matter (PM) emissions generated by diesel combustion have been causing a serious impact on human health and the environment [1]. The emission reduction requirements for fossil fuel combustion are becoming increasingly more stringent in order to reduce pollutants to protect the environment [2]. Cleaner combustion technologies especially fuels with minimal environmental impact and more effective combustion and emission control strategies should be developed to satisfy the stringent emission regulations.

Alternative fuels are thought to be effective in providing sustainable/renewable energy sources for engines to achieve high efficiency and clean combustion [3]. In recent years, the most frequently investigated alternative liquid fuels are alcohol, biodiesel, and dimethyl ether (DME) [4-9]. Polyoxymethylene dimethyl ethers (abbreviated as $PODE_n$, DMM_n, or OME_n) as an alternative fuel have attracted considerable interest recently [10-13]. The general chemical structure of OME_n is CH_3-O-$(CH_2$-O$)_n$-CH_3, where n is the number of oxymethylene units. A number of studies have shown that the addition of OME_n to diesel fuel could effectively reduce PM emissions due to its high oxygen content and absence of carbon-carbon bonds in the molecular structure [14-16]. The high cetane number of OME_n could also improve the anti-knock performance of the fuel [17]. Furthermore, OME_n is a sustainable and eco-friendly fuel which can be produced from biomass including waste biomass via syngas [18] and even from CO_2 [19].

Since blended fuels are often intended to be directly used in existing engines, the miscibility of different chemical substances in the mixture should be guaranteed when

evaluating if an alternative fuel can be used in practical engines. The fuel mixture formation has significant effects on the spray and combustion characteristics [7]. The inhomogeneity of blend fuel caused by poor miscibility will affect the fuel/air mixing, combustion and pollutant emissions, which can also offset the effect of the oxygenation of OME_n on reducing PM emissions. The unwanted phase separation of the fuel blends would affect the combustion stability, causing damage to the engine and making noise. Cylinder pressure, heat release, emissions, and fuel economy of OME_n/diesel blend were tested by Liu et al. [20]. The OME_n adopted in their work is a mixture of 2.6% OME_2, 88.9% OME_3, and 8.5% OME_4. There was no solubility issue when OME_n was blended with diesel at room temperature. The miscibility of OME_n with diesel was also studied by Han et al. [21]. The OME_n contains 20% OME_1, 24% OME_2, 25% OME_3, 17% OME_4 and 14% OME_{5-8}. They found that a mixture of OME_{3-8} and diesel had good solubility and stability. Jin et al. [22] investigated the phase behavior of OME_n and diesel mixture. The OME_n is composed of OME_3, OME_4, OME_5, and OME_6 with mass fractions of 45%, 28%, 17%, and 10% respectively. It was found that the OME_n can be blended with diesel fuel without phase separation when the ambient temperature is higher than 10°C. The blends have a relatively poor solubility at temperatures below 10°C. Moreover, OME_n has been used as a co-solvent for the blends of alcohol/diesel [22] and alcohol/soybean oil [23]. The experimental results showed that the OME_n has the ability to maintain the stability of the alcohol/diesel blend.

Although there are several experiments reported that the OME_n can be blended with diesel without causing major issues, it is believed that the number of oxymethylene units affects the miscibility. In addition, low-temperature performance can be a concern. Li et al. [24] investigated the solubility of OME_n/diesel blend, and the results showed that the cloud points of OME_{3-8}/diesel blend and OME_{3-5}/diesel blend are 7 °C and -11 °C, respectively. Omari et al. [25] also reported that blends of 35 vol% OME_n in diesel exhibit increasing cloud point temperatures with rising OME_n chain length. In addition, the OME_n adopted in the aforementioned experiments is a mixture of OME_{1-8}. Fundamental and comprehensive studies on the pure components of OME_n and diesel blends have been rarely carried out. Yang et. al [26] investigated the solubility of pure OME_{1-8} in six diesel hydrocarbons and three surrogate diesel fuels at different temperatures by using simulation software to predict the thermo-physical data of chemical compounds. They found that the solubility of pure OME_{1-8} in the diesel hydrocarbons and the surrogate diesel fuels decrease with the increasing number of oxymethylene units. It was also observed that the solubility of OME_n and diesel mixtures become worse when switching from fossil to paraffin diesel [25]. However, the mechanisms behind the change of solubility are largely unknown, while the understanding on this can help optimise fuel blend compositions. Presently, the intermolecular interaction between OME_n and

diesel molecules, including the types of paraffins and aromatics, have not been fully understood and further investigation is needed.

Analytical and computational methods including molecular dynamics (MD) are powerful means to conduct microscopic studies to investigate the underlying mechanisms of physicochemical processes of fuel mixtures. The MD simulation method is based on the numerical solution of Newton's laws of motion for all atoms of the system [27]. MD was already successfully applied to study the miscibility of the binary or ternary system [28-30]. Oliveira and Caires [31] investigated the molecular arrangement of the diesel/biodiesel blend by MD simulations. In another study, Oliveira et al. [32] adopted MD to study the effect of biodiesel as a co-solvent on the miscibility of diesel/ethanol blend. Pozar et al. [33] investigated the phase behavior of ethanol and alkanes, and they evaluated the different statistical methods to describe the morphological changes in the mixtures. Although MD has been proven to be an effective method in providing in-depth understanding at the molecular level, the mixture of OME_n/diesel has not been studied by using MD simulations. The effects of the number of methylene groups and ether groups on the intermolecular and intramolecular interaction are not fully understood.

This study was aimed at understanding the phase behavior of OME_n/diesel blend at the molecular level. A deeper understanding of the phase behavior will contribute to the utilisation of blended OME_n and diesel fuels to avoid fueling problems, to reduce pollutant emissions, and to resolve issues such as cold start of the engine. The fundamental understanding can provide guidance on solving the miscibility problem of OME_n and diesel blends, and on optimizing OME_n and diesel blend compositions in practical applications. As phase separation is essentially determined by the atomic-level interactions between different molecules, MD was used to gain insight into the miscibility of OME_n/diesel blend in this study. The miscibility of pure components of OME_{1-6}/diesel blends was studied. Although OME_{1-2} is considered not suitable for blending with diesel due to its low flash point and low viscosity [11], these components are often contained in the fuel mixtures. The OME_n adopted in the aforementioned experiments also contains OME_{1-2}. Besides, the investigation of the interaction between OME_{1-2} and diesel molecules can help reveal the mechanism of phase separation of OME_n/diesel blend. Intermolecular interactions, including the van der Waals (vdW) and electrostatic interactions, between OME_n and diesel molecules were analyzed. Effects of the molecular arrangement of OME_n and diesel mixtures were also studied. The rest of the paper is organised as follows. Section 2 presents the methodology. Section 3 presents results and discussions, focusing on the miscibility of OME_n/diesel blends, the intermolecular interactions, and the molecular arrangement of diesel around OME_n. Finally, Section 4 draws the conclusions of the study.

2. **Methodology**

2.1. Computational details

The diesel surrogate model adopted in this work was built by Oliveira et al. [32], which contains *n*-paraffins, *iso*-paraffins, naphthenes, aromatics, and heteroatomic molecules. The number of molecules was modified to maintain the same mass fraction of OME_n in the OME_n/diesel mixtures. There are 6 sets of blends, B1-B6. The mass fraction of OME_n is 20% for all the cases considered because the European Stationary Cycle test was conducted using 20% OME_n/diesel blends in heavy-duty engines as the reference for future applications [34]. The structures of diesel and OME_n are shown in Fig. 1, and the details of OME_n and diesel molecule number are listed in Table 1.

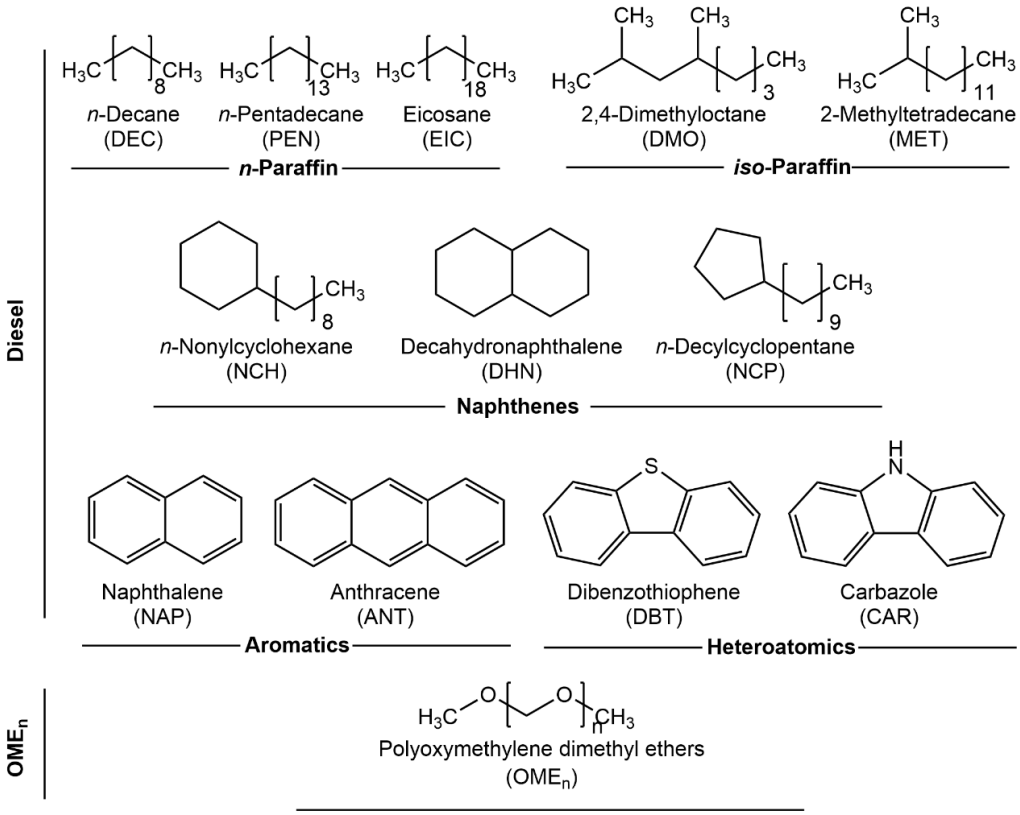

Fig. 1. Molecular structures of diesel and OME_n used in the simulations.

Table 1. Diesel and OME_n molecules used in the MD simulations

Class	Molecule name	Code ID	Molecules blend					
			B1	B2	B3	B4	B5	B6
n-Paraffins	*n*-Decane	DEC	150	150	150	150	150	150
	n-Pentadecane	PEN	60	60	60	60	60	60
	Eicosane	EIC	40	40	40	40	40	40
iso-Paraffins	2,4-Dimethyloctane	DMO	150	150	150	150	150	150
	2-Methyltetradecane	MET	60	60	60	60	60	60

Naphthenes	Decahydronaphthalene	DHN	140	140	140	140	140	140
	n-Nonylcyclohexane	NCH	90	90	90	90	90	90
	n-Decylcyclopentane	DCP	90	90	90	90	90	90
Aromatics	Naphthalene	NAP	90	90	90	90	90	90
	Anthracene	ANT	90	90	90	90	90	90
Heteroatomics	Dibenzothiophene	DBT	30	30	30	30	30	30
	Carbazole	CAR	30	30	30	30	30	30
			n=1	n=2	n=3	n=4	n=5	n=6
	Polyoxymethylene dimethyl ethers	OME_n	580	420	330	275	230	200

The MD simulations were performed by using Gromacs 2020 [35], which is an open-source package to perform molecular dynamics simulations. Gromacs is computationally effective at calculating the nonbonded interactions (that usually dominate simulations), and it has been widely used to investigate the solubility of blends [36-38]. The potential energy of aromatics, heteroatomic molecules, and OME_n were described by optimized potentials for liquid simulations all-atom (OPLS-AA) force field, which has been widely used in organic liquids simulations [39-41]. It should be noted that the acquisition of OPLS force field parameters for OME_n was based on OME_1. The molecular simulation accuracy of $OME_{2\text{-}6}$ by using OPLS force field will be discussed subsequently. The optimized OPLS force field for long hydrocarbons (LOPLS) [42] was used to model *n*-paraffins, *iso*-paraffins, and naphthenes. The form of the potential energy function for OPLS and LOPLS force field is given by the following equation [43]:

$$E = \sum_{bonds} K_r (r - r_{eq})^2 + \sum_{angles} K_\theta (\theta - \theta_{eq})^2 + \sum_{dihedrals} \sum_{l=1}^{3} K_l (1/2 - (-1)^l \cos l\varphi) + \sum_i \sum_{j>i} f_{ij} \left(4\varepsilon_{ij} \left((\sigma_{ij} / r_{ij})^{12} - (\sigma_{ij} / r_{ij})^6 \right) + q_i q_j e^2 / r_{ij} \right) \quad (1)$$

where K_r, K_θ, K_l are bond, angle, and dihedral force constants respectively. In Eq. (1), r represents the bond length between two atoms, θ is the angle of bond, and φ is the dihedral angle, while q, σ, ε are the atomic charges, the Lennard-Jones (L-J) radii, and the L-J well-depth respectively. Scaling factors f_{ij} =1.0 except for intramolecular 1,4-interactions for which f_{ij} =0.5 [43]. The combining rules $\sigma_{ij} = (\sigma_i \sigma_j)^{1/2}$ and $\varepsilon_{ij} = (\varepsilon_i \varepsilon_j)^{1/2}$ are used for the L-J energy interaction between different types of atoms. Subscript "eq" is the equilibrium value of bond and angle terms.

Initial configurations of $OME_{1\text{-}6}$/diesel blends were built by using Packmol [44]. Diesel and

OME_n molecules were constructed into a 100×100×100 Å cubic box with a lower initial density to avoid overlapping of atoms. The initial velocities for all atoms were generated randomly following the Maxwell-Boltzmann distribution. Energy minimization was carried out by using the steepest descent method first, followed by a 200 ps simulation in canonical ensemble (NVT) to remove the possible overlap between atoms. Finally, the simulation was run in the isothermal-isobaric ensemble (NPT) for 50 ns to obtain a reasonable density of the system. The size of the final simulation box is around 75×75×75 Å, which is dependent on the atom number and density of each system. The temperature and pressure for all simulations were 300 K and 1 bar.

The periodic boundary conditions were employed in all directions. Fast smooth Particle-Mesh Ewald summation [45] was used for the electrostatic interactions, and a cut off of 1.0 nm was used for the calculation of the van der Waals (vdW) interactions. All bonds associated with hydrogen atoms were constrained by using the linear constraint solver algorithm [46]. Velocity rescaling (v-rescale) method [47] was used to control the temperature, and Berendsen method [48] was applied for pressure coupling. A 2.0 fs time step was used, and output coordinates were obtained every 0.1 ps. The snapshots of trajectories were visualized by Visual Molecular Dynamics (VMD) [49]. Fig. 2 shows a snapshot of simulation system.

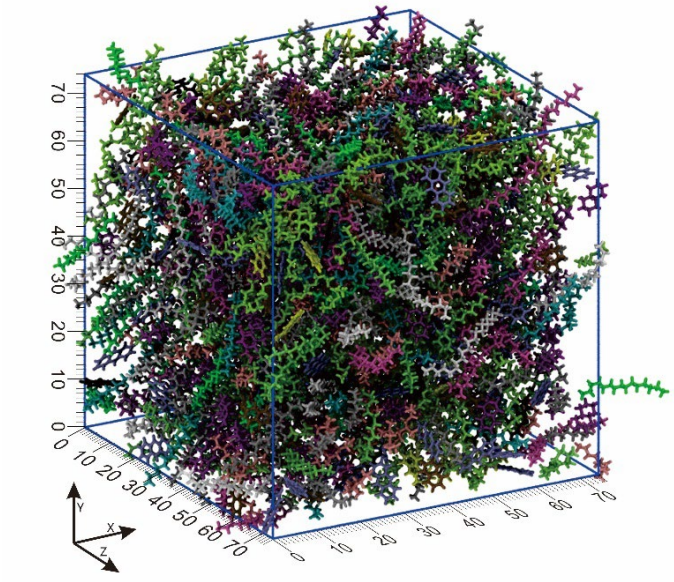

Fig. 2. Snapshot of simulation system. Molecules are colored for visual clarity.

2.2. Validation of simulation methods

The LOPLS force field parameters adopted in this work come from Shirley et al. [42]. Atomic partial charges for DBT and CAR were computed based on the 1.14*CM1A-LBCC charge model [50]. Liquid properties, including density, heat of vaporization, and molecular

volumes, are often used as yardsticks to verify the validity of the force fields [43, 51]. In this work, the liquid densities (ρ^{liq}) of pure components at each temperature were calculated to verify the validity of the OPLS and LOPLS force fields. Fig. 3(a) and Fig. 3(b) show the simulation density results for pure OME_{1-6} and their comparison to experimental data. The density results obtained with the OPLS force field show good agreement with the experimental data for OME_1 to OME_6, with average deviations less than 4% at 1 bar. Although the simulation slightly overestimated the densities especially for OME_{4-6} since the OPLS parameters for ethers were developed using OME_1. The deviation ranges are relatively small, and the trends are consistent with experimental data. Fig. 3(c) and Fig. 3(d) represent the simulation results of densities of diesel components and corresponding deviations between the experimental and the simulation results. The densities of paraffins (paraffins in this paper refer to *n*-paraffins and *iso*-paraffins) and naphthenes calculated by the LOPLS force field show good agreement with the experimental data, with average deviations less than 2.5% at 1 bar. The deviations for the density of DBT and CAR are ~3.5% and ~5.5% respectively, which are in the acceptable range. The results show that the OPLS and LOPLS force fields have the ability to describe the potential energy of diesel and OME_n. More information on the experimental and simulation data is given in the Supporting Information.

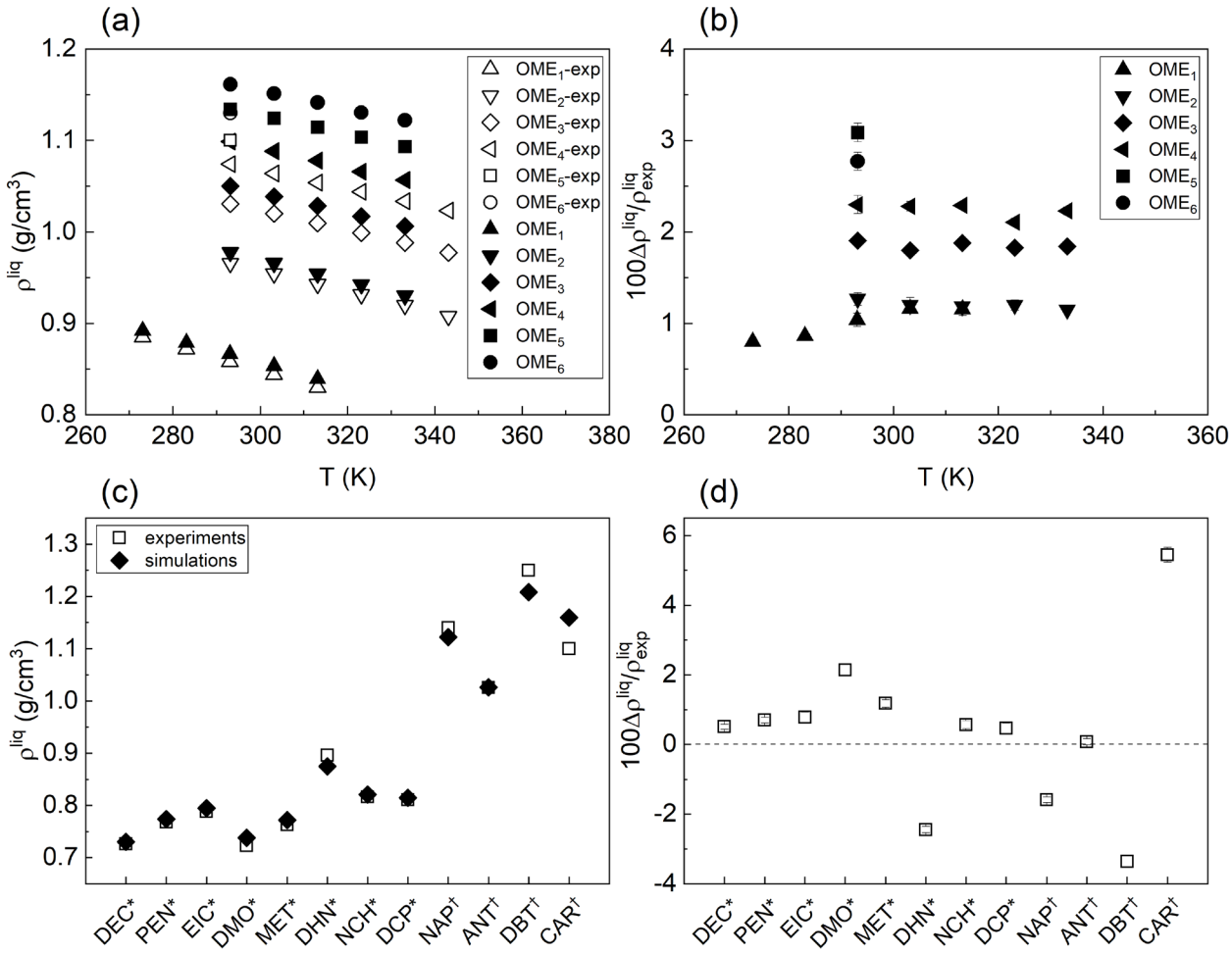

Fig. 3. Liquid densities for OME_{1-6} and diesel: (a) Densities of OME_{1-6} as a function of temperature; (b) Corresponding deviations between the experimental data (ρ_{exp}^{liq}) and the MD results for OME_{1-6}; (c) Experimental and simulation results for densities of diesel components; (d) Corresponding deviations between the experimental data and the MD results for diesel components. Experimental values are taken from the literature [3, 52-56]. Superscripts * and † represent molecules described by LOPLS and OPLS force field respectively.

3. Results and discussion

3.1. Miscibility of OME_{1-6}/diesel blends

The composition of diesel is complex, including various paraffins, naphthenes, aromatics, and heteroatomic molecules, which makes the interactions between diesel and OME_n rather complicated. The snapshots of OME_{1-6} molecules in B1-B6 blends at 0 ns, 10 ns, 20 ns, 30 ns, and 50 ns are presented in Fig. 4. It can be observed that OME_{1-6} molecules were evenly distributed over the whole simulation box at the initial stage. However, the distribution of OME_{1-6} evolved differently over time. The molecules of OME_1 and OME_2 were distributed evenly in the box at 50 ns. Although OME_3 molecules aggregated with each other to a certain degree,

they were distributed in the entire space. The OME_{4-6} started aggregate with each other at 10 ns, and the degree of aggregation of OME_{5-6} is higher than that of OME_4. The molecular aggregation of OME_{4-6} in these blends is obvious after 20 ns. Most of the OME_{4-6} molecules were concentrated in specific areas, and only a small part of the molecules was scattered in other spaces after 30 ns. Although OME_{4-6} molecules were mingled with some diesel molecules, the distribution shows that the miscibility of OME_{4-6}/diesel blends is lower than that of OME_{1-3}/diesel blends. In previous experimental studies [20, 21], the OME_n can be blended with diesel well at room temperature when the mass fraction of OME_{1-3} in OME_n reaches 80-90%. The blends of OME_n/diesel blends have a relatively poor solubility when the mass fraction of OME_{4-6} is increased to 55% as reported in an early study [22]. The simulation results are consistent with experimental observations.

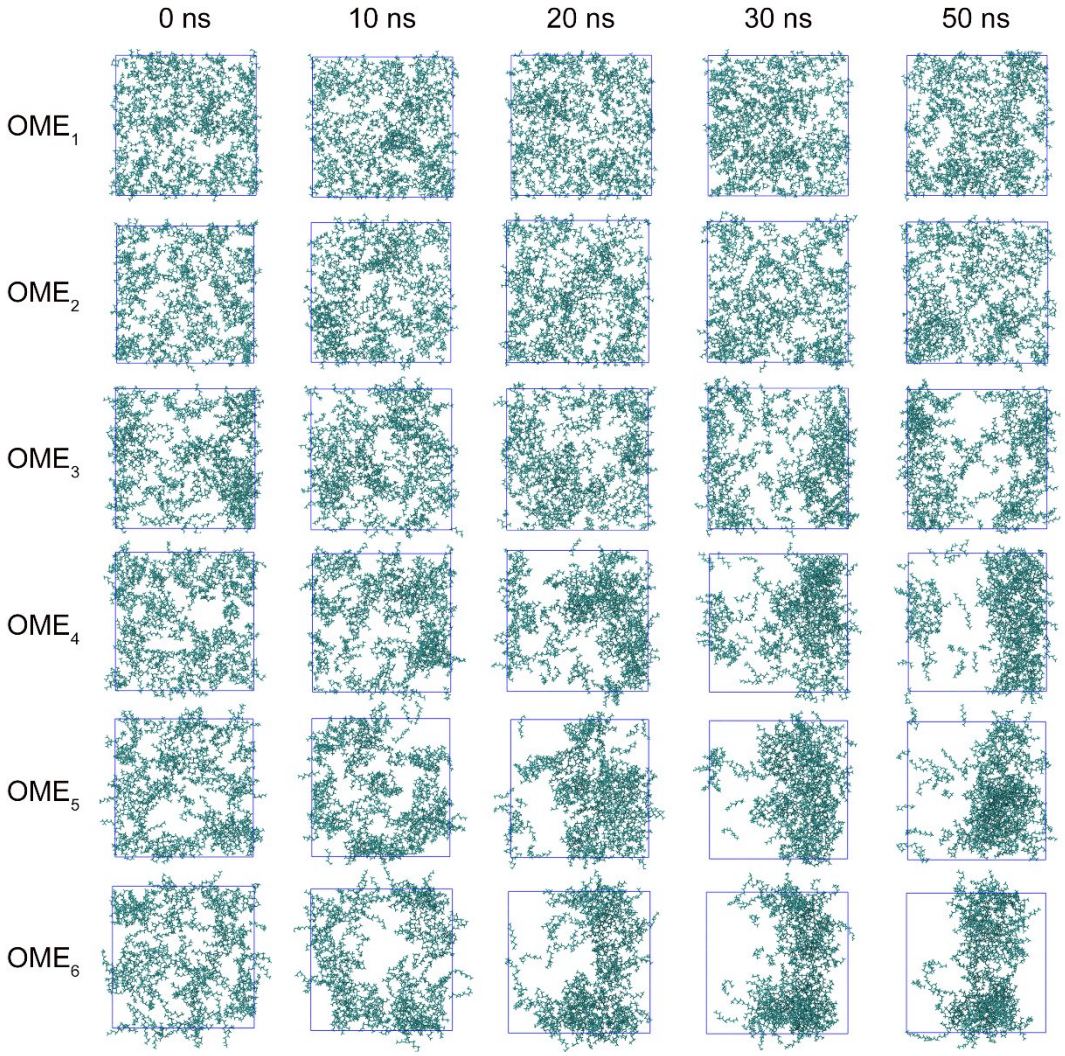

Fig. 4. Snapshots of OME_{1-6} molecule distributions at different times. Diesel molecules have been hidden for clarity.

The phase separation as a function of time was described by the “demixing index” χ_{demix},

which was proposed by Muzet et al. [57] to study the phase separation of binary water-chloroform mixtures. It has been widely used to describe the phase separation of binary mixtures [58, 59]. The blend of diesel and OME_n can be regarded as a binary mixture, where χ_{demix} was calculated from the coordinates of all atoms. The whole simulation box was divided into n cubic boxes with a length of 10 Å. The density of every single box (ρ_i) was computed using $1/\rho_i = 1/\rho_{d,i} + 1/\rho_{o,i}$ based on the densities of diesel ($\rho_{d,i}$) and OME_n ($\rho_{o,i}$). The "demixing index" was obtained from the average over all boxes ($\chi_{demix} = \langle \rho_i \rangle$) and normalized in such a way that χ_{demix} ranges from 1.0 (homogeneous system) to 0.0 (two nonoverlapping separated phases).

The demixing index χ_{demix} of B1-B6 blends over time is reported in Fig. 5. The χ_{demix} for OME_1/diesel and OME_2/diesel fluctuated between 0.95 and 1, which suggests that the OME_1 and OME_2 molecules were distributed evenly throughout the box during the whole simulation process. It was shown that OME_1 and OME_2 can be blended with diesel very well. The χ_{demix} for OME_3/diesel blend decreased slightly during 0 to 20 ns and then fluctuated around 0.90. OME_3 molecules aggregate with each other to a certain degree when OME_3 is evenly distributed in the blends by molecular interactions. Such aggregation would not lead to phase separation of OME_3/diesel blend as shown in Fig. 4. This means that OME_3 also has good solubility with diesel. Similar trends were found in OME_4/diesel, OME_5/diesel, and OME_6/diesel blends. The significant decrease in χ_{demix} for OME_4/diesel, OME_5/diesel, and OME_6/diesel blends is a reflection of the phase separation. The rate and degree of decrease are faster and greater with the increase of oxymethylene units, which demonstrates that the miscibility of OME_n/diesel blends decreases with the increase of oxymethylene units.

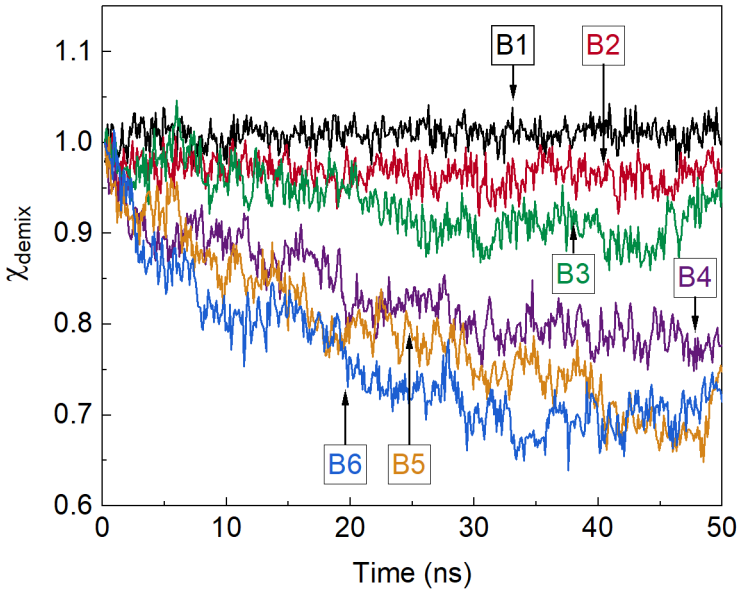

Fig. 5. Evolution of the demixing index of B1-B6 system.

In order to investigate the molecular distribution of OME_n and diesel when phase separation occurred, the snapshots of OME_6 and diesel components at 50 ns are presented in Fig. 6. OME_6/diesel blend was chosen to study the molecule distribution due to its high degree of phase separation. It can be seen that the regions with higher local density of OME_6 showed a low density of *n*-paraffins, *iso*-paraffins, and naphthenes, indicating that these molecules are separated from OME_6 molecules. The molecules of aromatics were relatively uniform in the blend, suggesting that the distribution of aromatics is independent of other molecules. The distribution of heteroatomic molecules, *i.e.,* DBT and CAR are closely related to OME_6. These molecules were accumulated around OME_6, especially for CAR. Although the distribution of DBT is related to OME_6, there were some DBT molecules scattered in the simulation box. The OME_6 has good miscibility with aromatic and heteroatomics molecules. Therefore, the miscibility of OME_n and diesel increases with the fraction of aromatic and heteroatomics components. This observation can explain the experimental results reported by Omari et al. [25] that the miscibility of OME_n and paraffin diesel blends is worse than OME_n and fossil diesel mixtures.

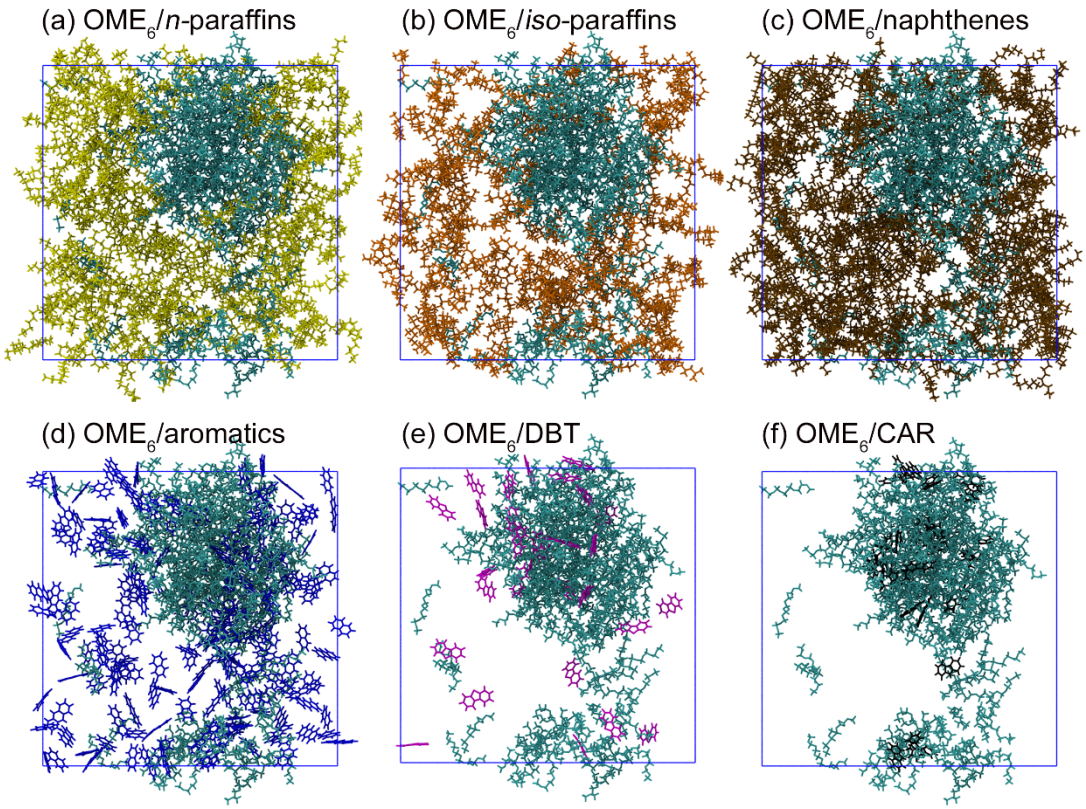

Fig. 6. Snapshots of OME_6 and diesel components at 50 ns, OME_6 is colored cyan: (a) OME_6/*n*-paraffins, *n*-paraffins are colored yellow, containing DEC, PEN, and EIC; (b) OME_6/*iso*-paraffins, *iso*-paraffins are colored orange, containing DMO and MET; (c) OME_6/naphthenes, naphthenes are colored ochre, containing DHN, NCH, and DCP; (d) OME_6/aromatics, aromatics are colored blue, containing NAP and ANT; (e) OME_6/DBT, DBT is colored magenta; (f) OME_6/CAR, CAR is colored black.

3.2. The intermolecular interactions

Intermolecular interactions are the interactions between two or more molecules. The interactions determine the physical and chemical properties of substances and the stability of chemical complexes [60]. The stability of OME_n/diesel blends would be good if the intermolecular interactions between these molecules in the fuel blends are strong. The investigation of intermolecular interactions between different molecules can offer a clear picture of why the miscibility of OME_n/diesel blend becomes worse with the increase of oxymethylene units. The intermolecular interactions are described by the non-bonded interactions between molecules, which is a combination of vdW and electrostatic potential energy. It should be noted that non-bonded interactions also exist between the atoms that belong to the same molecule. This part should be removed when we calculate the intermolecular interactions by using the total non-bonded interactions in Gromacs.

3.2.1. OME_n intermolecular interactions

In order to gain a deeper insight into the reasons that lead to the increase of intermolecular interactions, the potential energy between molecules needs to be studied. Given that the intermolecular interactions measured in Gromacs depend on the molecule number, while the number of OME_n is varying in B1-B6 blends to ensure the same mass fraction of OME_n. The potential energy was averaged by molecule number for comparison. The vdW (U_{vdW}) and electrostatic ($U_{electrostatic}$) potential energy of single OME_n molecules are shown in Fig. 7 (a) and Fig. 7 (b) respectively. Fig. 7 (c) represents the proportion of $U_{electrostatic}$ in total intermolecular interaction (U_{total}). It should be noted that the potential energy mentioned here only contains the intermolecular potential energy between OME_n molecules, which excludes the energy between OME_n and diesel molecules.

It can be observed that the U_{vdW} and $U_{electrostatic}$ between OME_n decrease with the increase of oxymethylene unit, and the negative values imply that there is an attractive interaction between OME_n molecules, as shown in Fig. 7 (a) and Fig. 7 (b). The decrease in potential energy represents the increase of intermolecular forces. The phase separation would occur when such attractive force grows to a certain extent. OME_{4-6} molecules aggregate to each under the combined effect of vdW and electrostatic interactions. The intermolecular forces between OME_{1-2} are too weak to maintain a stable cluster. The U_{vdW} and $U_{electrostatic}$ for OME_{4-6} all experienced varying degrees of decrease over 50 ns, which is because the distance between atoms decreases during the aggregation process. The proportion of the $U_{electrostatic}$ increases with the oxymethylene units as shown in Fig. 7 (c). For instance, the proportion increases from 22.7% to 30.0% when the oxymethylene unit increases from 1 to 6. It can be deducted that the phase separation of OME_n/diesel is governed by vdW and electrostatic interactions, and the importance of electrostatic interaction grows with the increase of oxymethylene units.

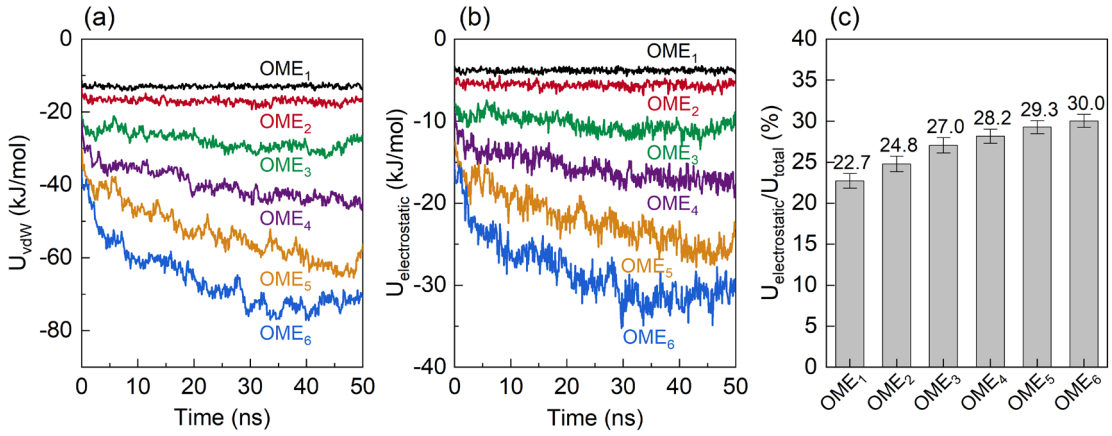

Fig. 7. The potential energy of OME_n molecules in B1-B6 blends over time: (a) VdW

potential energy of OME_{1-6} over time; (b) Electrostatic potential energy of OME_{1-6} over time; (c) The proportion of electrostatic potential energy in total intermolecular potential energy.

The electrostatic interaction plays an important role in the aggregation process of OME_n. The impact of ether and methylene groups on the $U_{electrostatic}$ is examined through the analysis of the contribution of each atom to the $U_{electrostatic}$, as shown in Fig. 8. The oscillation of the atoms in the equilibrium position would affect the magnitude of the $U_{electrostatic}$. The $U_{electrostatic}$ is positive for oxygen atoms, and negative for carbon and hydrogen atoms most of the time. This is because the electronegativity of oxygen is larger than carbon. The charges for oxygen, carbon, and hydrogen in the oxymethylene unit are -0.4e, +0.2e, +0.1e respectively. The attractive interaction between ether and methylene groups is stronger than the repulsive interaction between methylene groups and the repulsive interaction between ether groups. Therefore, the attractive interaction between ether and methylene groups would promote the aggregation of OME_n molecules. Meanwhile, the $U_{electrostatic}$ of oxygen would increase with oxymethylene units, but such increment is smaller than the decrement in the $U_{electrostatic}$ of methylene groups. It can be deduced that the increase of electrostatic interactions between OME_n molecules is mainly from the attractive force between ether and methylene groups. The electrostatic force between the ether groups will have a repulsive effect, but such force is less than the overall attractive force.

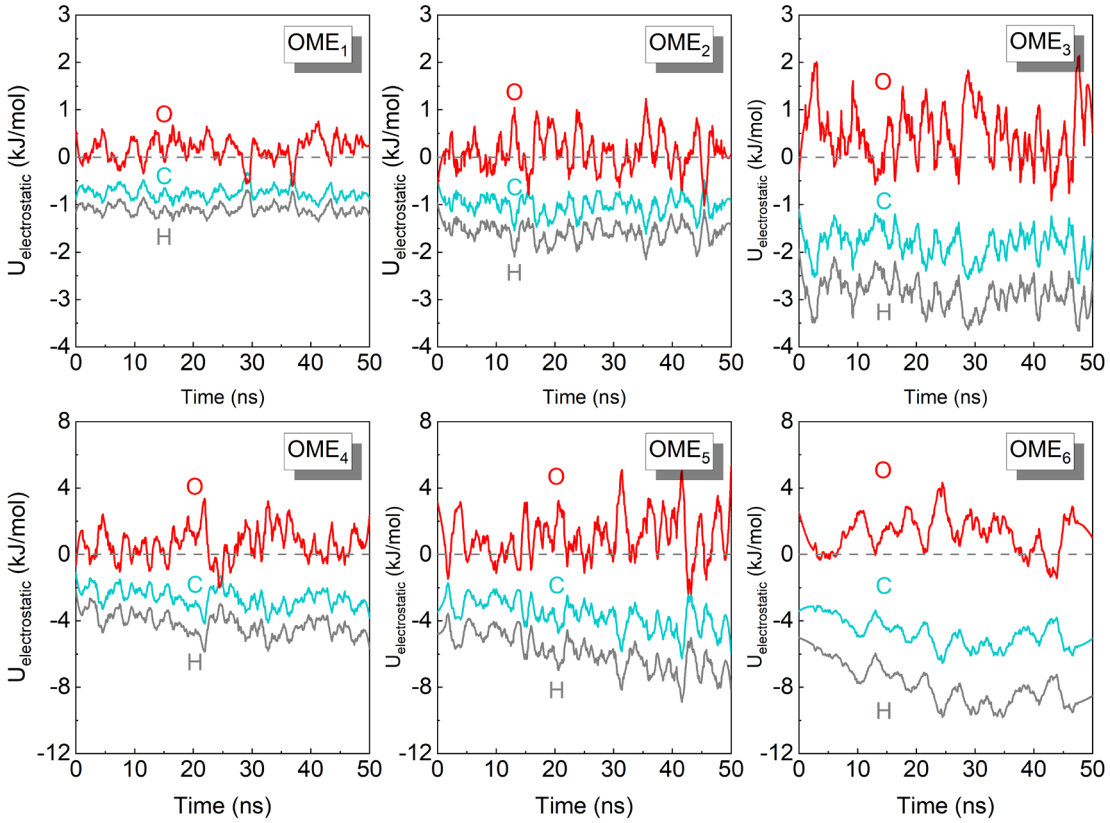

Fig. 8. The contribution of each atom to the $U_{electrostatic}$ between OME_{1-6} molecules. Carbon, oxygen, and hydrogen atoms are represented by C, O, and H respectively. The red, cyan, and grey line represent the $U_{electrostatic}$ evolution of carbon, oxygen, and hydrogen atoms.

3.2.2. OME_n/diesel intermolecular interactions

The intermolecular potential energy between OME_6 and diesel molecules is presented in Fig. 9. The potential energy is averaged by the molecule number of corresponding component. It can be seen that the U_{vdW} for those molecules aggregated with each other decreases over time, such as OME_6/DBT and OME_6/CAR. The separation leads to increased vdW interactions, such as OME_6/DEC. Other diesel components that separated from OME_6 showed similar characteristics to OME_6/DEC, as presented in Fig. S1. The U_{vdW} for OME_6/CAR is smaller than that of OME_6/DBT, which indicates that there is a relatively strong vdW interaction between OME_6 and CAR molecules. Electrostatic interaction also plays a significant role in the miscibility of diesel and OME_n mixture. Among all the diesel components, OME_6/CAR exhibits the lowest $U_{electrostatic}$. Meanwhile, the proportion of $U_{electrostatic}$ in total potential energy for OME_6/CAR is also the highest (41%) as shown in Fig. 9 (c). The $U_{electrostatic}$ of OME_6/DBT (-10 kJ/mol) is higher compared to OME_6/CAR, accounting for 22.4 % of the total intermolecular potential energy. Although the U_{vdW} difference for OME_6/CAR and OME_6/DBT is small as shown in Fig. 9 (a), the difference in $U_{electrostatic}$ makes the miscibility of OME_6/CAR better than

that of OME_6/DBT. The same trend can be found between OME_6/DEC and OME_6/NAP. The U_{vdW} for OME_6/DEC and OME_6/NAP are both around -20 kJ/mol at initial stage. Lower $U_{electrostatic}$ enables NAP distributing uniformly in the blend, while DEC is separated from OME_6 as presented in Fig. 6. It can be deduced that the distribution of OME_n and diesel molecules are determined by the vdW and electrostatic interactions. The $U_{electrostatic}$ differences of OME_n and other diesel components are huge. Diesel components that can form high electrostatic interaction with OME_n tend to have good miscibility with OME_n. Therefore, OME_n has good miscibility with the diesel that has a high fraction of aromatic components [26].

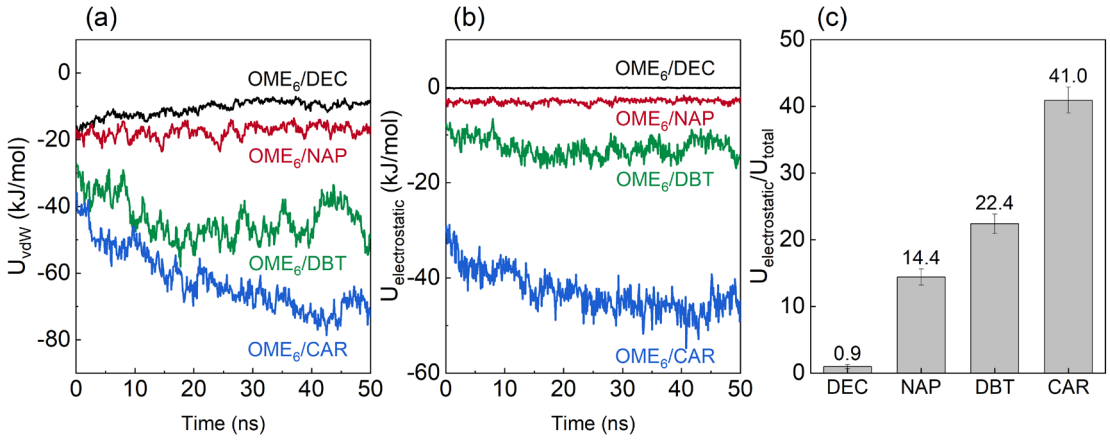

Fig. 9. The potential energy between OME_6 and diesel molecules : (a) The vdW potential energy between OME_6 and diesel molecules over time; (b) Electrostatic potential energy between OME_6 and diesel molecules over time; (c) The proportion of electrostatic potential energy in total intermolecular potential energy.

The atomic contributions of diesel molecules to the $U_{electrostatic}$ between OME_6 and diesel are presented in Fig. 10. The $U_{electrostatic}$ for carbons are highly correlated with hydrogen atoms. This is because almost all the hydrogen atoms are bonded with carbon, except for the hydrogen atoms bonded with nitrogen (HN) in CAR, the movement of carbon and hydrogen atoms are consistent. The attractive interaction of hydrogen atoms is counteracted by the repulsive interaction of carbon in OME_6/DEC, which leads to the low electrostatic interaction of OME_6/DEC. Same situation also occurs for other *n*-paraffins and *iso*-paraffins molecules, as shown in Fig. S2. It was found that the $U_{electrostatic}$ for methyl or methylene units nearly approach zero, which indicates the structure of the methyl or methylene group is detrimental to the formation of electrostatic interaction with other molecules. The attractive interaction of hydrogen in NAP, DBT, and CAR is higher than the repulsive interaction of carbon, which is due to the planar structure of these molecules.

The electrostatic interaction between diesel and OME_6 molecules does not depend on the molecular structure only, but also relies on the electronegativity difference of atoms in

diesel molecules. The diesel molecules will have a strong electrostatic interaction with OME_6 if the former have atoms with a relatively large positive charge. For example, the average charge for hydrogen in NAP and DBT is +0.115 e and +0.14 e respectively, which leads to the electrostatic interaction of OME_6/DBT being larger than that of OME_6/NAP. Due to the high electronegativity of nitrogen, the charge for the hydrogen atom bonded with nitrogen atom is +0.45 e, which has the lowest $U_{electrostatic}$ as shown in Fig. 10. HN will form hydrogen bonds with the oxygen atoms in OME_n. Meanwhile, the nitrogen also captures the electrons of carbons, resulting in the positive charge of adjacent carbon. The strong electrostatic interaction between OME_n molecules also can be attributed to the electronegativity difference of oxygen and carbon atoms. It can be concluded that the electrostatic interaction between diesel and OME_n molecules depends on the molecular structure of diesel molecules and the electronegativity differences of atoms in diesel molecules.

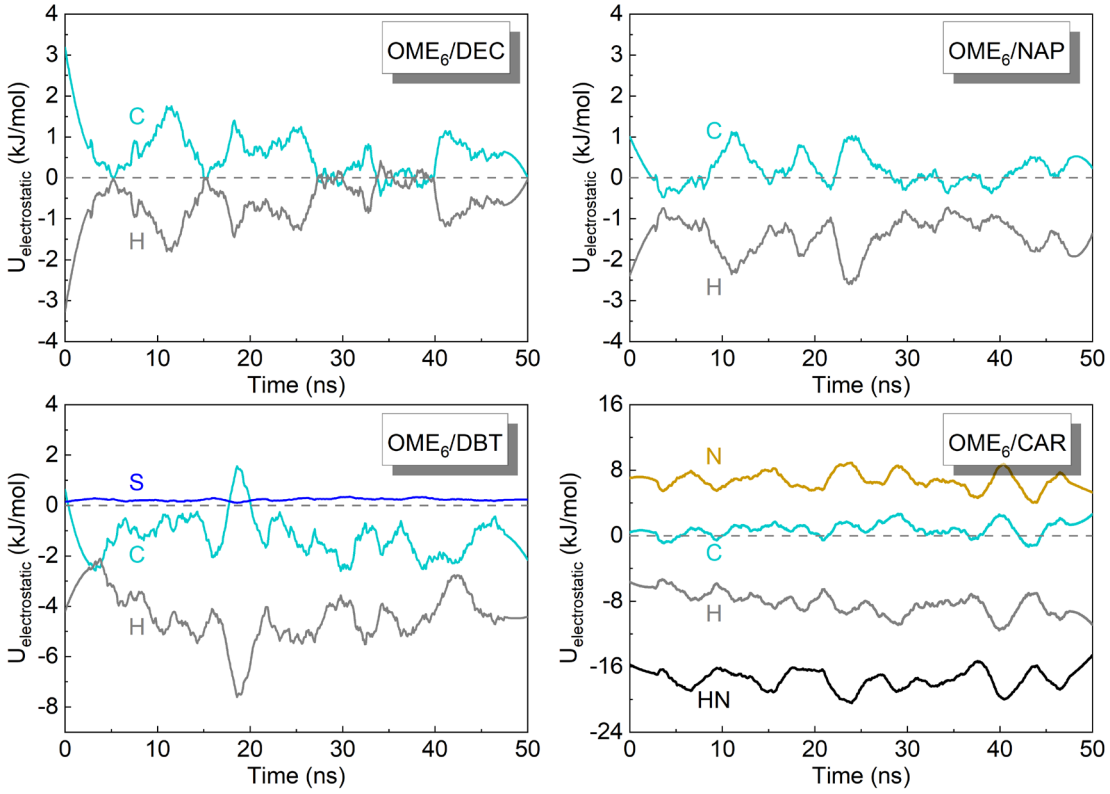

Fig. 10. The atomic contribution of diesel molecules to the $U_{electrostatic}$ between OME_6 and diesel molecules. Carbon, nitrogen, sulfur, hydrogen atoms bonded with carbon, and hydrogen atom bonded with nitrogen are represented by C, N, S, H, HN respectively. The cyan, yellow, blue, grey, and black line represent the $U_{electrostatic}$ evolution of carbon, nitrogen, sulfur, hydrogen atoms bonded with carbon, and hydrogen atom bonded with nitrogen respectively.

3.3. The molecular arrangement of diesel around OME_n

The minimum-distance distribution function $g^{md}(r)$ was adopted in this work to study the molecular arrangement of diesel around OME_n. This function was proposed by Martínez and Shimizu [61] to study the solute−solvent interactions. It has been used to study diesel and biodiesel systems [31, 32]. Standard radial distribution functions g(r) cannot be directly used in the study of the solvation of complex, nonspherical solutes. The difference between g(r) and $g^{md}(r)$ is that the former considers the distance between the center mass of the molecules, while the latter considers the minimum distance between solute-solvent. The minimum-distance distribution function $g^{md}(r)$ can be obtained using the method of Martínez and Shimizu [61], which was computed by using ComplexMixtures [62] in this study.

Fig. 11 shows the distribution of the DEC, DMO, and DHN molecules around the $OME_{1\text{-}6}$ molecules at 50 ns. The DEC, DMO, and DHN presented a similar profile of distribution around the $OME_{1\text{-}6}$ molecules because of their molecular similarities. The maximum $g^{md}(r)$ decreased with the increase of oxymethylene units. For example, the $g^{md}(r)$ for OME_1/DEC is ~4.24, and this value decreased to ~2.38 for OME_6/DEC. This is due to the separation between OME_n and DEC when the number of oxymethylene units is more than 3. The peak of $g^{md}(r)$ was observed at ~2.36 Å to ~2.37 Å for all cases, which is because the equilibrium distance between atoms depends on the value of σ in L-J potential [63]. The outermost layers of paraffins and naphthenes are hydrogen atoms, and the values of σ are the same. Therefore, the distributions of DEC, DMO, and DHN molecules around the $OME_{1\text{-}6}$ molecules at the separation interface are similar. The other alkanes components of diesel show a similar $g^{md}(r)$ (Fig. S3). Consequently, the present findings show that the chain length and structures (straight, branched, and ring) of alkanes have little impact on the molecular distribution around OME_n.

(a)

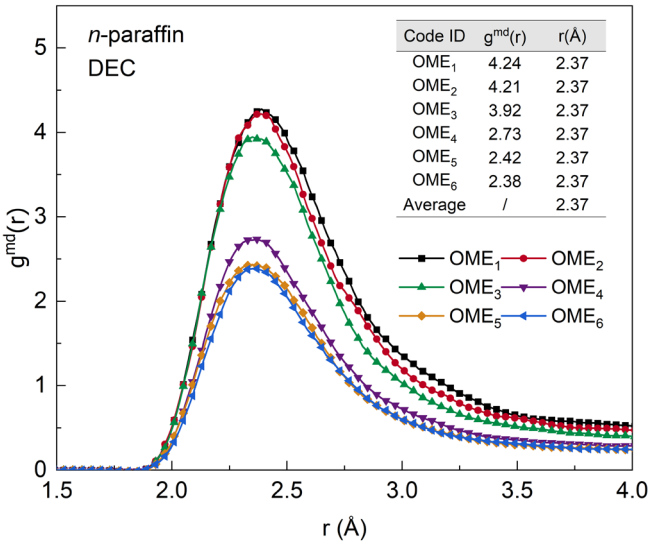
n-paraffin
DEC
Code ID g^md(r) r(Å)
OME1 4.24 2.37
OME2 4.21 2.37
OME3 3.92 2.37
OME4 2.73 2.37
OME5 2.42 2.37
OME6 2.38 2.37
Average / 2.37
OME1 OME2
OME3 OME4
OME5 OME6
g^md(r)
r (Å)

(b)

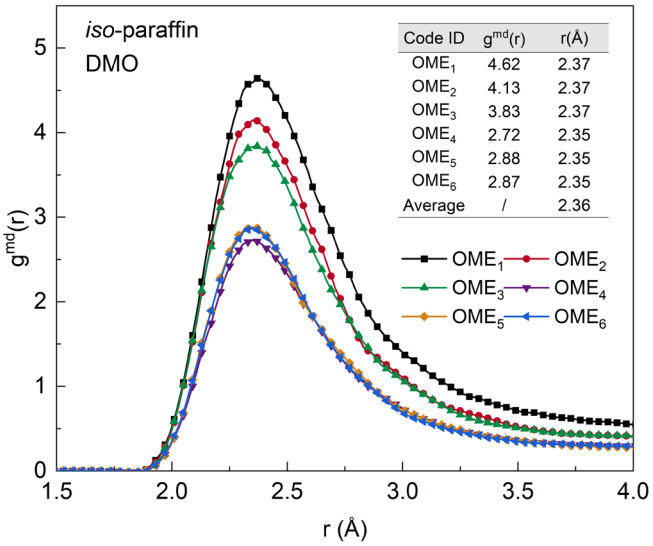
iso-paraffin
DMO
Code ID g^md(r) r(Å)
OME1 4.62 2.37
OME2 4.13 2.37
OME3 3.83 2.37
OME4 2.72 2.35
OME5 2.88 2.35
OME6 2.87 2.35
Average / 2.36
OME1 OME2
OME3 OME4
OME5 OME6
g^md(r)
r (Å)

(c)

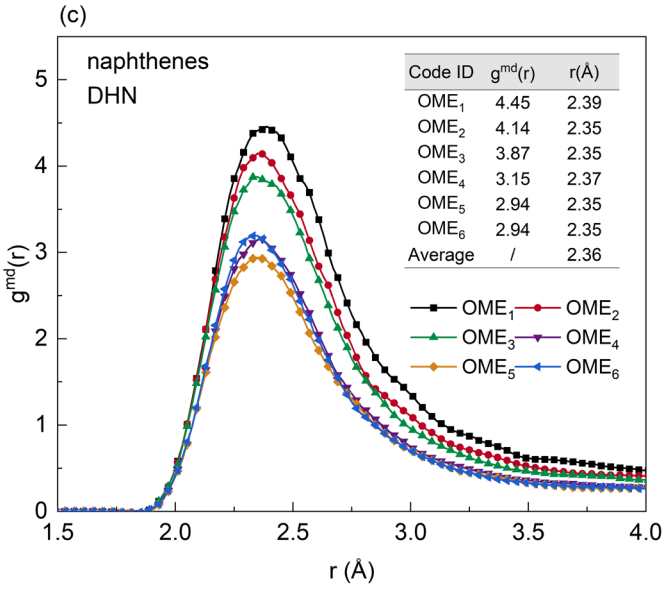
naphthenes
DHN
Code ID g^md(r) r(Å)
OME1 4.45 2.39
OME2 4.14 2.35
OME3 3.87 2.35
OME4 3.15 2.37
OME5 2.94 2.35
OME6 2.94 2.35
Average / 2.36
OME1 OME2
OME3 OME4
OME5 OME6
g^md(r)
r (Å)

Fig. 11. The distribution of the diesel molecules (solvent) around the OME_{1-6} molecules (solute) at 50 ns for the: (a) DEC, (b) DMO, and (c) DHN. The values of $g^{md}(r)$ and r listed in the tables are the maximum $g^{md}(r)$ and corresponding distance.

The distribution of the NAP, DBT, and CAR molecules around the OME_{1-6} molecules at 50 ns is presented in Fig. 12. There is no clear dependence of oxymethylene units on the accumulation of NAP around the OME_{1-6} since the NAP molecules were distributed evenly in B1-B6 blends as discussed before. The maximum $g^{md}(r)$ for OME_n/CAR increased with oxymethylene units, which is due to the increasing local density of CAR around OME_n. A maximum concentration at ~2.47 Å, ~2.54 Å, and ~2.53 Å was observed for NAP, DBT, and CAR respectively, which is higher than that of OME_n/paraffins and OME_n/naphthenes. This is due to the fact that the structures of aromatics and heteroatomic molecules are planar, and the closest atoms near OME_n could be hydrogen atoms or other atoms. Thus, it can be suggested that the molecular arrangement of diesel around OME_n depends on the molecular structure.

The atomic contribution of NAP, DBT, and CAR to $g^{md}(r)$ of OME_6 including hydrogen (H), carbon (C), sulfur (S), and nitrogen (N) atoms, are presented in Fig. 13. A high concentration of hydrogen atoms at ~2.4 Å was observed. Carbon, sulfur, and nitrogen atoms peaked at ~2.8 Å. The values of σ in L-J potential for carbon, sulfur, and nitrogen atoms are higher than that of hydrogen atoms. Therefore, the equilibrium distances between OME_n and these atoms are larger. In addition, the maximum $g^{md}(r)$ for hydrogen atoms are higher than other atoms, which reveals that the OME_n molecules tend to combine with the hydrogen atoms in aromatics and heteroatomic molecules. It is interesting to note that a peak at ~1.8 Å was observed for CAR, which is related to the orientation of hydrogen bonds.

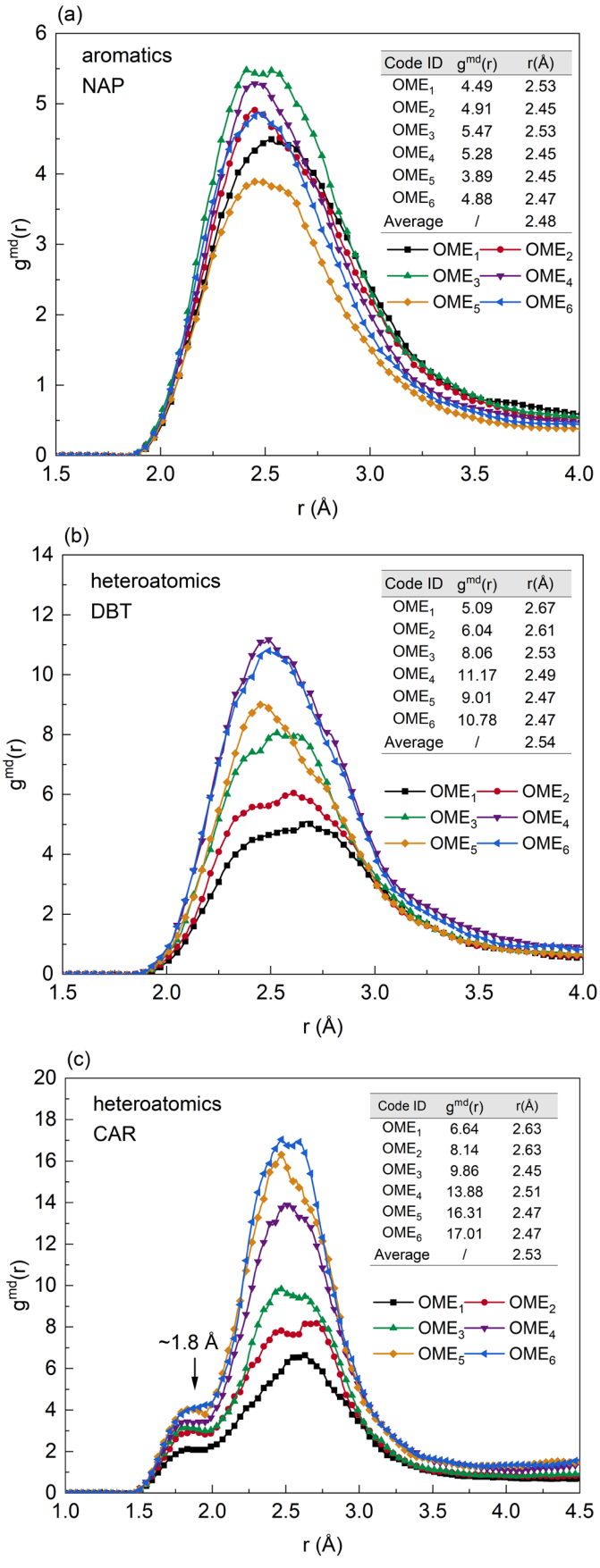
(a)
aromatics
NAP
Code ID g^md(r) r(Å)
OME1 4.49 2.53
OME2 4.91 2.45
OME3 5.47 2.53
OME4 5.28 2.45
OME5 3.89 2.45
OME6 4.88 2.47
Average / 2.48
OME1 OME2 OME3 OME4 OME5 OME6
g^md(r)
r (Å)
(b)
heteroatomics
DBT
Code ID g^md(r) r(Å)
OME1 5.09 2.67
OME2 6.04 2.61
OME3 8.06 2.53
OME4 11.17 2.49
OME5 9.01 2.47
OME6 10.78 2.47
Average / 2.54
OME1 OME2 OME3 OME4 OME5 OME6
g^md(r)
r (Å)
(c)
heteroatomics
CAR
Code ID g^md(r) r(Å)
OME1 6.64 2.63
OME2 8.14 2.63
OME3 9.86 2.45
OME4 13.88 2.51
OME5 16.31 2.47
OME6 17.01 2.47
Average / 2.53
~1.8 Å
OME1 OME2 OME3 OME4 OME5 OME6
g^md(r)
r (Å)

Fig. 12. The distribution of the diesel molecules (solvent) around the $OME_{1\text{-}6}$ molecules (solute) for the: (a) NAP, (b) DBT, and (c) CAR. The values of $g^{md}(r)$ and r listed in the tables are the maximum $g^{md}(r)$ and the corresponding distance in each case.

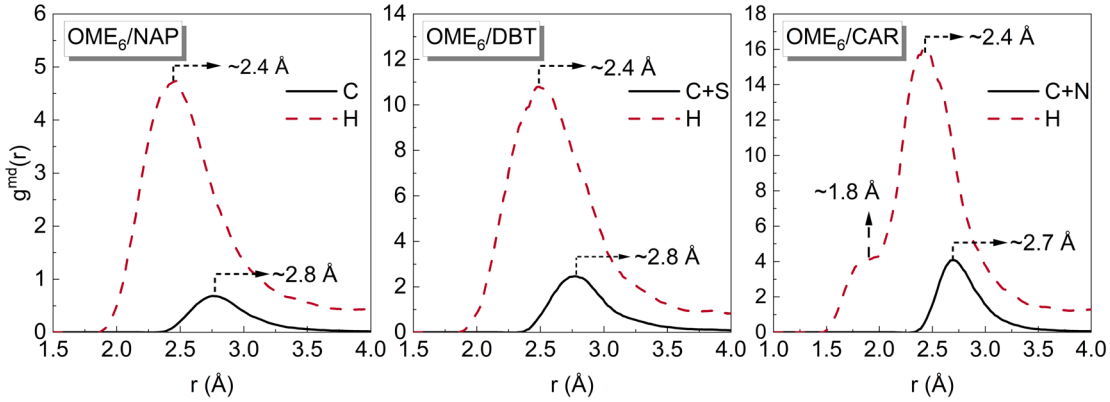

Fig. 13. The atomic contribution of NAP, DBT, and CAR (solvent) to $g^{md}(r)$ of OME_6 (solute). Hydrogen, carbon, sulfur, and nitrogen atoms in solvent molecules are represented by H, C, S, and N respectively. The red dash line represents the contribution of hydrogen atoms, and the black solid line is the contribution of other atoms.

4. Conclusions

The miscibility of polyoxymethylene dimethyl ethers and diesel blends at 300 K and 1 atm has been studied using molecular dynamics simulation. Various analyses have been conducted to determine the aggregation and separation behavior of OME_n and diesel molecules. It is found that the miscibility of OME_n and diesel decreases with the increasing number of oxymethylene units. The paraffins and naphthenes in diesel tend to separate with OME_n molecules, while the heteroatomic molecules are prone to accumulate around OME_n. The distribution of aromatics is independent of OME_n molecules. The aromatics and heteroatomic molecules help maintain the stability of OME_n/diesel blends, but their negative impact on pollutant formation of diesel combustion also needs to be taken into account in practical applications.

The analyses of the intermolecular interactions between OME_n and diesel molecules show that the increasing vdW and electrostatic interaction contribute to the aggregation of OME_n and eventually lead to phase separation of OME_n/diesel blends. Electrostatic interaction plays a significant role in the liquid-liquid equilibrium of OME_n/diesel blends. Those types of molecules having strong electrostatic interaction with OME_n tend to accumulate around OME_n, while those with low electrostatic interaction molecules would separate from OME_n. Planar molecular structure and large electronegativity differences of atoms in diesel molecules would lead to the high electrostatic interaction. Molecules containing the polar functional groups and

long carbon chains, such as biodiesel or long chain alcohol, have the potential to be used as an additive to stabilize the diesel and OME_n blends.

Minimum-distance distribution functions were used to determine the molecular arrangement of diesel molecules around the OME_n molecules, showing that the paraffins and naphthenes preferentially accumulate at a distance of ~2.36 Å from the surface of the OME_n. The chain structure and chain length of alkanes have little impact on the molecular distribution around OME_n. Compared to carbon, sulfur, and nitrogen atoms, the OME_n molecules tend to combine with the hydrogen atoms of aromatics and heteroatomic molecules at a distance of ~2.4 Å. This study provides a molecular basis for the interpretation of the OME_n/diesel interactions, which can be used to help optimise fuel blend compositions.

Acknowledgement

The computing resources were provided by the UK Consortium on Mesoscale Engineering Sciences (UKCOMES) supported by EPSRC under EP/R029598/1.

References

[1] Neer A, Koylu U. Effect of operating conditions on the size, morphology, and concentration of submicrometer particulates emitted from a diesel engine. *Combustion and Flame* 2006;146(1-2):142-54.

[2] Agarwal AK, Mustafi NN. Real-world automotive emissions: Monitoring methodologies, and control measures. *Renewable and Sustainable Energy Reviews* 2021;137:110624.

[3] Liu J, Wang H, Li Y, Zheng Z, Xue Z, Shang H, et al. Effects of diesel/PODE (polyoxymethylene dimethyl ethers) blends on combustion and emission characteristics in a heavy duty diesel engine. *Fuel* 2016;177:206-16.

[4] Ghadikolaei MA, Wong PK, Cheung CS, Ning Z, Yung K-F, Zhao J, et al. Impact of lower and higher alcohols on the physicochemical properties of particulate matter from diesel engines: A review. *Renewable and Sustainable Energy Reviews* 2021;143:110970.

[5] Kumar S, Cho JH, Park J, Moon I. Advances in diesel-alcohol blends and their effects on the performance and emissions of diesel engines. *Renewable and Sustainable Energy Reviews* 2013;22:46-72.

[6] Geng P, Cao E, Tan Q, Wei L. Effects of alternative fuels on the combustion characteristics and emission products from diesel engines: A review. *Renewable and Sustainable Energy Reviews* 2017;71:523-34.

[7] Jiang Z, Gan Y, Ju Y, Liang J, Zhou Y. Experimental study on the electrospray and combustion characteristics of biodiesel-ethanol blends in a meso-scale combustor. *Energy* 2019;179:843-9.

[8] Zhou Y, Gan Y, Gou X. Chemical kinetic modeling study of methyl esters oxidation: Improvement on the prediction of early CO_2 formation. *Fuel* 2020;279:118383.

[9] Zhou Y, Gan Y, Zhang C, Shi D, Jiang Z, Luo Y. Numerical study for influence of ozone on the

combustion of biodiesel surrogates in a homogeneous charge compression ignition engine. *Fuel Processing Technology* 2022;225:107039.

[10] Burger J, Siegert M, Ströfer E, Hasse H. Poly(oxymethylene) dimethyl ethers as components of tailored diesel fuel: Properties, synthesis and purification concepts. *Fuel* 2010;89(11):3315-9.

[11] Awad OI, Ma X, Kamil M, Ali OM, Ma Y, Shuai S. Overview of polyoxymethylene dimethyl ether additive as an eco-friendly fuel for an internal combustion engine: Current application and environmental impacts. *Science of The Total Environment* 2020;715:136849.

[12] He J, Chen H, Su X, Xie B, Li Q. Combustion study of polyoxymethylene dimethyl ethers and diesel blend fuels on an optical engine. *Energies* 2021;14(15):4608.

[13] Zhu Q, Zong Y, Yu W, Yang W, Kraft M. Understanding the blending effect of polyoxymethylene dimethyl ethers as additive in a common-rail diesel engine. *Applied Energy* 2021;300:117380.

[14] Palazzo N, Zigan L, Huber FJT, Will S. Impact of oxygenated additives on soot properties during diesel combustion. *Energies* 2020;14(1):147.

[15] Preuß J, Munch K, Denbratt I. Performance and emissions of renewable blends with OME_{3-5} and HVO in heavy duty and light duty compression ignition engines. *Fuel* 2021;303:121275.

[16] Härtl M, Seidenspinner P, Jacob E, Wachtmeister G. Oxygenate screening on a heavy-duty diesel engine and emission characteristics of highly oxygenated oxymethylene ether fuel OME_1. *Fuel* 2015;153:328-35.

[17] Lautenschütz L, Oestreich D, Seidenspinner P, Arnold U, Dinjus E, Sauer J. Physico-chemical properties and fuel characteristics of oxymethylene dialkyl ethers. *Fuel* 2016;173:129-37.

[18] Zhang X, Kumar A, Arnold U, Sauer J. Biomass-derived oxymethylene ethers as diesel additives: A thermodynamic analysis. *Energy Procedia* 2014;61:1921-4.

[19] Held M, Tönges Y, Pélerin D, Härtl M, Wachtmeister G, Burger J. On the energetic efficiency of producing polyoxymethylene dimethyl ethers from CO_2 using electrical energy. *Energy & Environmental Science* 2019;12(3):1019-34.

[20] Liu H, Wang Z, Wang J, He X, Zheng Y, Tang Q, et al. Performance, combustion and emission characteristics of a diesel engine fueled with polyoxymethylene dimethyl ethers ($PODE_{3-4}$)/ diesel blends. *Energy* 2015;88:793-800.

[21] Han D, Cao Z, Shi W, Deng X, Yang T. Influence of polyoxymethylene dimethyl ethers on diesel fuel properties. *Energy Sources, Part A: Recovery, Utilization, and Environmental Effects* 2016;38(18):2687-92.

[22] Jin C, Zhang X, Wang X, Xiang Y, Cui X, Yin Z, et al. Effects of polyoxymethylene dimethyl ethers on the solubility of ethanol/diesel and hydrous ethanol/diesel fuel blends. *Energy Science & Engineering* 2019;7(6):2855-65.

[23] Jin C, Zhang X, Geng Z, Pang X, Wang X, Ji J, et al. Effects of various co-solvents on the solubility between blends of soybean oil with either methanol or ethanol. *Fuel* 2019;244:461-71.

[24] Li X, Yu H, Sun Y, Wang H, Guo T, Sui Y, et al. Synthesis and application of polyoxymethylene dimethyl ethers. *Applied Mechanics and Materials* 2014;448:2969-73.

[25] Omari A, Heuser B, Pischinger S, Rüdinger C. Potential of long-chain oxymethylene ether and oxymethylene ether-diesel blends for ultra-low emission engines. *Applied Energy* 2019;239:1242-9.

[26] Yang Z, Ren C, Jiang S, Xin Y, Hu Y, Liu Z. Theoretical predictions of compatibility of polyoxymethylene dimethyl ethers with diesel fuels and diesel additives. *Fuel* 2022;307:121797.

[27] Komanduri R, Raff LM. A review on the molecular dynamics simulation of machining at the atomic

scale. *Proceedings of the Institution of Mechanical Engineers, Part B: Journal of Engineering Manufacture* 2001;215(12):1639-72.

[28] Luo Z, Jiang J. Molecular dynamics and dissipative particle dynamics simulations for the miscibility of poly (ethylene oxide)/poly (vinyl chloride) blends. *Polymer* 2010;51(1):291-9.

[29] Gupta J, Nunes C, Vyas S, Jonnalagadda S. Prediction of solubility parameters and miscibility of pharmaceutical compounds by molecular dynamics simulations. *The Journal of Physical Chemistry B* 2011;115(9):2014-23.

[30] Ghazipour H, Gutiérrez A, Mohammad-Aghaie D, Alavianmher MM, Hosseini SM, Aparicio S. Insights on biodiesel blends with alkanol solvents. *Journal of Molecular Liquids* 2021;332:115864.

[31] Oliveira IPd, Caires ARL. Molecular arrangement in diesel/biodiesel blends: A molecular dynamics simulation analysis. *Renewable Energy* 2019;140:203-11.

[32] Oliveira IPd, Caires ARL, Baskar K, Ponnusamy S, Lakshmanan P, Veerappan V. Biodiesel as an additive for diesel-ethanol (diesohol) blend: physical-chemical parameters and origin of the fuels' miscibility. *Fuel* 2020;263:116753.

[33] Požar M, Lovrinčević B, Zoranić L, Primorać T, Sokolić F, Perera A. Micro-heterogeneity versus clustering in binary mixtures of ethanol with water or alkanes. *Physical Chemistry Chemical Physics* 2016;18(34):23971-9.

[34] Liu H, Wang Z, Zhang J, Wang J, Shuai S. Study on combustion and emission characteristics of Polyoxymethylene Dimethyl Ethers/diesel blends in light-duty and heavy-duty diesel engines. *Applied Energy* 2017;185:1393-402.

[35] Bekker H, Berendsen H, Dijkstra E, Achterop S, Vondrumen R, Vanderspoel D, et al. Gromacs-a parallel computer for molecular-dynamics simulations. *4th International Conference on Computational Physics (PC 92).* World Scientific Publishing; 1993:252-6.

[36] Chandran P, Shah JK. A molecular simulation approach to the computation of mutual solubility of water and organic liquids: Application to fatty acids. *Fluid Phase Equilibria* 2018;472:48-55.

[37] Vermaas JV, Crowley MF, Beckham GT. Molecular lignin solubility and structure in organic solvents. *ACS Sustainable Chemistry & Engineering* 2020;8(48):17839-50.

[38] Zhang J, Seyyedi M, Clennell MB. Molecular dynamics simulation of transport and structural properties of CO_2-alkanes. *Energy & Fuels* 2021;35(8):6700-10.

[39] Chen C, Jiang X. Transport property prediction and inhomogeneity analysis of supercritical n-Dodecane by molecular dynamics simulation. *Fuel* 2019;244:48-60.

[40] Garrido NM, Jorge M, Queimada AJ, Gomes JRB, Economou IG, Macedo EA. Predicting hydration Gibbs energies of alkyl-aromatics using molecular simulation: A comparison of current force fields and the development of a new parameter set for accurate solvation data. *Physical Chemistry Chemical Physics* 2011;13(38):17384.

[41] Sonibare K, Rathnayaka L, Zhang L. Comparison of CHARMM and OPLS-aa forcefield predictions for components in one model asphalt mixture. *Construction and Building Materials* 2020; 236: 117577.

[42] Shirley WIS, Pluhackova K, Böckmann RA. Optimization of the OPLS-AA force field for long hydrocarbons. *Journal of Chemical Theory and Computation* 2012;8(4):1459-70.

[43] Jorgensen WL, Maxwell DS, Tirado-Rives J. Development and testing of the OPLS all-atom force field on conformational energetics and properties of organic liquids. *Journal of the American Chemical Society* 1996;118(45):11225-36.

[44] Martínez L, Andrade R, Birgin EG, Martínez JM. PACKMOL: A package for building initial

configurations for molecular dynamics simulations. *Journal of Computational Chemistry* 2009;30(13):2157-64.

[45] Darden T, York D, Pedersen L. Particle mesh Ewald: An N·log(N) method for Ewald sums in large systems. *The Journal of Chemical Physics* 1993;98(12):10089-92.

[46] Hess B, Bekker H, Berendsen HJC, Fraaije JGEM. LINCS: A linear constraint solver for molecular simulations. *Journal of Computational Chemistry* 1997;18(12):1463-72.

[47] Bussi G, Donadio D, Parrinello M. Canonical sampling through velocity rescaling. *The Journal of Chemical Physics* 2007;126(1):014101.

[48] Berendsen HJC, Postma JPM, Van Gunsteren WF, Dinola A, Haak JR. Molecular dynamics with coupling to an external bath. *The Journal of Chemical Physics* 1984;81(8):3684-90.

[49] Humphrey W, Dalke A, Schulten K. VMD: Visual molecular dynamics. *Journal of Molecular Graphics* 1996;14(1):33-8.

[50] Dodda LS, Vilseck JZ, Tirado-Rives J, Jorgensen WL. 1.14*CM1A-LBCC: Localized bond-charge corrected CM1A charges for condensed-phase simulations. *The Journal of Physical Chemistry B* 2017;121(15):3864-70.

[51] Kulkarni A, García EJ, Damone A, Schappals M, Stephan S, Kohns M, et al. A force field for poly(oxymethylene) dimethyl ethers (OME_n). *Journal of Chemical Theory and Computation* 2020;16(4):2517-28.

[52] Wang X, Pan J, Wu J, Liu Z. Surface tension of dimethoxymethane and methyltert-butyl ether. *Journal of Chemical & Engineering Data* 2006;51(4):1394-7.

[53] Burger J, Ströfer E, Hasse H. Production process for diesel fuel components poly(oxymethylene) dimethyl ethers from methane-based products by hierarchical optimization with varying model depth. *Chemical Engineering Research and Design* 2013;91(12):2648-62.

[54] Lide DR. Handbook of chemistry and physics. Internet Version 2005 ed. Boca Raton: CRC press; 2005.

[55] O'Neil MJ. the Merck Index: An Encyclopedia of Chemicals, Drugs,and Biologicals. 15th ed. Cambridge, UK: Royal Society of Chemistry; 2013.

[56] Yaws CL. Thermophysical properties of chemicals and hydrocarbons. William Andrew; 2008.

[57] Muzet N, Engler E, Wipff G. Demixing of binary water−chloroform mixtures containing ionophoric solutes and ion recognition at a liquid−liquid interface: A molecular dynamics study. *The Journal of Physical Chemistry B* 1998;102(52):10772-88.

[58] Biswas R, Ghosh P, Banerjee T, Ali SM, Singha Deb AK. Interfacial behavior of Cs+, K+, Na+, and Rb+extraction in the presence of Dibenzo-18-Crown-6 from the Nitrobenzene–water biphasic system: Experimental, quantum chemical, and molecular dynamic studies. *ACS Omega* 2018;3(2):1663-74.

[59] Baaden M, Burgard M, Wipff G. TBP at the water−oil interface: The effect of TBP concentration and water acidity investigated by molecular dynamics simulations. *The Journal of Physical Chemistry B* 2001;105(45):11131-41.

[60] Kaplan IG. Intermolecular interactions: physical picture, computational methods and model potentials. John Wiley & Sons; 2006.

[61] Martínez L, Shimizu S. Molecular interpretation of preferential interactions in protein solvation: A solvent-shell perspective by means of minimum-distance distribution functions. *Journal of Chemical Theory and Computation* 2017;13(12):6358-72.

[62] Martínez L. ComplexMixtures.jl: Investigating the structure of solutions of complex-shaped

molecules from a solvent-shell perspective. *Journal of Molecular Liquids* 2021:117945.

[63] Cheng Z, Xu W, Tang L. Theory and practice of molecular modeling. Beijing: Chemical Industry Press; 2007.